Biological Cybernetics (2019) 113:71–82
https://doi.org/10.1007/s00422-018-0778-6

Biological Cybernetics

ORIGINAL ARTICLE

Cellular switches orchestrate rhythmic circuits

Guillaume Drion[1] · Alessio Franci[2] · Rodolphe Sepulchre[3]

Received: 15 February 2018 / Accepted: 20 August 2018 / Published online: 3 September 2018

Abstract
Small inhibitory neuronal circuits have long been identified as key neuronal motifs to generate and modulate the coexisting rhythms of various motor functions. Our paper highlights the role of a cellular switching mechanism to orchestrate such circuits. The cellular switch makes the circuits reconfigurable, robust, adaptable, and externally controllable. Without this cellular mechanism, the circuit rhythms entirely rely on specific tunings of the synaptic connectivity, which makes them rigid, fragile, and difficult to control externally. We illustrate those properties on the much studied architecture of a small network controlling both the pyloric and gastric rhythms of crabs. The cellular switch is provided by a slow negative conductance often neglected in mathematical modeling of central pattern generators. We propose that this conductance is simple to model and key to computational studies of rhythmic circuit neuromodulation.

Keywords Central pattern generators · Neuromodulation · Mathematical modeling

1 Introduction

The ability of the simplest organisms to orchestrate basic rhythmic motor functions such as breathing, chewing, swallowing, walking, or heart beating has long fascinated scientists and engineers. On the one hand, those functions have many of the attributes of autonomous clocks, suggesting that they could easily be emulated by machines. On the other hand, the adaptability and resilience of those rhythmic functions in the animal world remain to date a mystery when compared to our most advanced robots. This paradox was a central drive from the early days of cybernetics, as exemplified for instance in the homeostat of Ashby and his concept of ultrastability (Ashby 1952). It remains a central question to date and was for instance heavily debated during the recent workshop on Control and Modulation of Neuronal and Motor Systems at the Mathematical Biosciences Institute. The contrast between animal and machine performance at orchestrating motor rhythms permeated much of the discussions and was equally underlined by neurophysiologists and roboticists.

This is not to say that no progress has been achieved since the days of the homeostat. Both the physiology and the mathematical modeling of rhythmic circuits are far better understood today than seventy years ago. Detailed anatomical and physiological studies of specific rhythms in specific animals have identified core neuronal mechanisms and circuit architectures that govern rhythmic functions. The concept of central pattern generators has replaced the concept of ultrastable machines and provides a quantitative link between the neurophysiology of animal circuits and the mathematical models used to engineer rhythmic machines, see e.g., Grillner (2003), Marder and Bucher (2007) and Ijspeert (2014). The core circuit architecture of central pattern generators is an

Communicated by Peter J. Thomas.

Guillaume Drion and Alessio Franci have contributed equally to this work.

This article belongs to the Special Issue on *Control Theory in Biology and Medicine.* It derived from a workshop at the Mathematical Biosciences Institute, Ohio State University, Columbus, OH, USA.

✉ Guillaume Drion
gdrion@uliege.be

Alessio Franci
afranci@ciencias.unam.mx

Rodolphe Sepulchre
r.sepulchre@eng.cam.ac.uk

[1] Department of Electrical Engineering and Computer Science, University of Liege, Liege, Belgium

[2] Department of Mathematics, Science Faculty, National Autonomous University of Mexico, Coyoacán, D.F., México

[3] Department of Engineering, University of Cambridge, Cambridge, UK

inhibitory coupling between a limited number of interneurons. Each neuron of the circuit has two distinct states of electrical activity (low and high firing rate) that resemble the on and off state of a discrete automaton. The transition times between on and off states in each neuron are constrained by the circuit topology, which generates specific circuit rhythms via specific phase shifts between the neuronal rhythms. The core mechanisms of such *rhythm boxes* have been extensively studied, both experimentally and computationally. The simplest such circuit is an anti-phase rhythm between two symmetrically coupled inhibitory neurons, known as the half-center oscillator (HCO). Neurophysiologists have identified the specific ionic currents underlying the rebound mechanisms that generate the circuit rhythm (Marder and Bucher 2001; Hill et al. 2003). Mathematical models of central pattern generators capture the phase properties of the circuits with highly simplified phase models for each neuron (Ijspeert et al. 2007). Such models have been instrumental in the development of robots that mimic animal locomotion such as Ijspeert et al. (2007) and Ijspeert (2014). Collectively, those efforts have provided a comprehensive modeling framework that accounts for the biophysical principles of autonomous clocks in neuronal circuits.

How the autonomous clocks can be orchestrated with the level of adaptability and resilience found in animals remains a largely debated experimental and modeling question. Central pattern generators, whether responsible for breathing, chewing, swallowing, walking or heart beating, all adapt their rhythm possibly in fractions of a second in reaction to the internal animal needs (e.g., choking prevention) or to unexpected external contingencies (e.g., predator escape). Growing experimental evidence suggests that such fast adaptation of rhythmic control might happen at the cellular level, that is, without affecting synaptic strength and the circuit interconnection topology (Marder and Bucher 2007; Harris-Warrick 2011). The role of neuromodulation has been under increasing scrutiny in recent years. The coordination of breathing, walking, and chewing critically relies on the modulation of inhibitory interneuron excitability via monoaminergic inputs (Jordan and Slawinska 2011; Dai and Jordan 2010; Liu et al. 2009; Harris-Warrick and Cohen 1985; Gordon and Whelan 2006). More generally, neuromodulators seem to play an important role in the control of circuits via the recruitment of individual inhibitory interneurons, governing their switch from low firing activity to rhythmic bursting (McLean et al. 2008; Berkowitz et al. 2010; Zhong et al. 2011; White and Nusbaum 2011).

Those recent experimental developments motivate the modeling question of this paper. We explore how a neuromodulatory control at the cellular level can contribute to orchestrating the rhythms of a circuit for a given connectivity. In particular, we aim at proposing a simple cellular mechanism by which the functional connectivity of a circuit is highly reconfigurable independently of its synaptic connectivity, consistently with recent experimental observations (Rodriguez et al. 2013; Marder et al. 2014, 2015; Daur et al. 2016). The proposed cellular mechanism provides an alternative to synaptic-based circuit rhythm modulation (Gutierrez et al. 2013) because it is entirely grounded in an intrinsic property of the interneurons: the presence of a slow negative conductance that can be activated by external neuromodulators. A negative conductance means a conductance with a negative gain $\frac{\delta I}{\delta V} < 0$ in some voltage range. In electronics, such circuit elements are called negative resistance devices. In neurophysiology, the gain of a conductance is time dependent, so that it can change sign over time. Typically, a sodium conductance has a negative gain in the fast timescale of channel activation but a positive gain in the slow timescale of inactivation. We call such a conductance *fast negative* and *slow positive*. A calcium conductance has similar properties but with a slow activation and ultraslow inactivation. We call such a conductance *slow negative* and *ultraslow positive*. The role of this specific intrinsic property has been extensively studied by the authors in the recent years (Dethier et al. 2015; Franci et al. 2018; Drion et al. 2018). It acts as a switch of excitability for the neuron. When the slow negative conductance is on, the excitability of the neuron is prone to slow rhythms characterized by prolonged bursts of high-frequency firing. When the slow negative conductance is off, the excitability of the neuron is only prone to the fast rhythms characteristic of individual spikes. The distinctive role of the slow negative conductance is not the generation of slow rhythms per se but rather to enable robust control and tunability of such slow rhythms. This is why it is often overlooked in computational models that concentrate on rhythm generation rather than rhythm regulation.

In previous work, we have shown the role of the slow negative conductance in single-cell control (Franci et al. 2018), in half-center oscillator control (Dethier et al. 2015), and in the control of large excitatory–inhibitory populations (Drion et al. 2018). Here, we want to explore the role of the same slow negative conductance in orchestrating small inhibitory circuits. We use a conceptual circuit model derived after the crab somatogastric ganglion (STG) connectivity diagram (Fig. 1b, left) (Gutierrez et al. 2013). This circuit model was developed to study the interaction between two different rhythms that coexist within the same circuit. In the STG, these two rhythms are the fast pyloric rhythm, which is constantly active, and the slow gastric mill rhythm, which can be turned on and off by afferent neuromodulatory inputs and neuromodulators (Marder and Bucher 2007). These two rhythms are carried on by neurons that share numerous synaptic connections, and many neurons switch between both rhythms or even synchronize with both rhythms at the same time (Gutierrez et al. 2013; Bucher et al. 2006; Dickinson et al. 1990; Meyrand et al. 1991; Weimann and Marder 1994)

Our results show that a slow negative conductance endows each cell of the circuit with a switching mechanism that governs their individual participation in the circuit rhythm and that is externally controlled by neuromodulators. We contrast the controllability properties of the circuit in the presence and in the absence of the cellular switch. A weakly interconnected circuit with switchable neurons is shown to be robust, adaptable, and reconfigurable. The synaptic connectivity constrains the phase relationships between the neurons, as in the classical models of central pattern generators. But the participation of each neuron in the orchestra is controlled externally and allows for a continuous and robust modulation of the circuit rhythms. The distinctive property of the slow negative conductance is that it only controls the switch but does not constrain the rhythm. In this manner, our model suggests a way to reconcile the clock properties of an autonomous rhythm box with the adaptation and resilience properties of rhythmic motor functions. We propose that the cellular switching mechanism can be easily incorporated in abstract computational models of central pattern generators and that it is important to account for this distinctive feature when studying the modulation and controllability properties of a rhythmic circuit.

2 Results

2.1 A source of cellular slow negative conductance is critical for the coexistence of switchable rhythms within a same circuit

Throughout this paper, we analyze a specific circuit model composed of five interconnected neurons. Neurons 1, 2 and neurons 4, 5 are, respectively, connected through mutually inhibitory synapses (Fig. 1a). Each pair of neurons generates the anti-phase rhythmic activity of a half-center oscillator (HCO). Following the approach of (Gutierrez et al. 2013), the HCO composed of neurons 1, 2 is designed to generate a fast and continuously active, pyloric-like rhythm (blue traces), whereas the HCO composed of neurons 4, 5 is designed to generate a slow, gastric mill-like rhythm that is only active under the action of specific neuromodulators (NMD) (red traces). Neuron 3 is a hub neuron, connected to both HCOs through electrical and chemical synapses as in Fig. 1b, left.

The dynamics of each neuron were modeled using two variants of the STG neuron conductance-based model described in Liu et al. (1998). This model is composed of seven voltage-gated currents, two of which are sources of a slow negative conductance (the two slowly activating calcium currents I_{CaT} and I_{CaS}). In the first variant (called the *original model*), the kinetics originally described in Liu et al. (1998) were used, making the modulation of the cellular slow negative conductance possible through the modulation of calcium channel density (Franci et al. 2018; Drion et al. 2015). In the second variant (called the *restorative variant*), the activation of both types of calcium channels were made ten times faster. This modification did not affect the steady-state properties of the model, both models having identical IV curves for any given parameter set. The slow negative conductance is, however, lost in the restorative variant because the two calcium conductances are now sources of fast rather than slow negative conductance. The meaning of *fast* and *slow* is relative to the kinetics of sodium activation (time constant ~ 0.5 ms close to spike threshold), here considered as *fast*. In the original version of the model, the kinetics of calcium activation is ten times slower than the kinetics of sodium activation, whereas the two distinct timescales are merged in the restorative variant. The reader is referred to Franci et al. (2018) for a detailed analysis of the dynamical consequences of this difference at the single-cell level.

First, we analyzed the ability to generate fast and slow rhythms in isolated, symmetrical, and homogenous HCOs (i.e., with no connection to the hub neuron) via different mechanisms (Fig. 1a). A numerical parameter space exploration shows that many different parameter combinations can lead to HCO rhythms. This parametric redundancy is well documented (see e.g., Prinz et al. 2003).

The circuit rhythms can, however, be grouped into two categories according to whether their origin is primarily cellular or synaptic. On the one hand, fast and slow HCOs can be generated by exploiting the cellular sources of slow negative conductance: The presence of a slow negative conductance at the cellular level makes the cells prone to engage in a circuit rhythmic activity, even for very weak synaptic connections (Fig. 1a, center). This *cellular mechanism* is accessible to all neurons or models that possess at least one source of slow negative conductance (i.e., one slowly activating inward current or one slowly inactivating outward current). Yet it has not received a lot of attention until very recently, even in the context of HCO rebound mechanisms (Dethier et al. 2015).

On the other hand, HCOs can be generated in the absence of any cellular slow negative conductance using strong synaptic connections. The synaptic connection strength in Fig. 1a right is ten times the synaptic connection strength in Fig. 1a center. This *circuit mechanism* is well known and has been extensively studied in the past (Marder and Bucher 2001; Hill et al. 2003). It is the only mechanism that can be used to build HCOs made of neuron models lacking any source of slow negative conductance, which includes any detailed conductance-based model with fast/instantaneous calcium activation (Terman et al. 2002; Rubin and Terman 2004; Butera et al. 1999; Golomb and Amitai 1997) and simple spiking neuron models such as the FitzHugh–Nagumo model (FitzHugh 1961) and integrate-and-fire models (Gerstner et al. 2014).

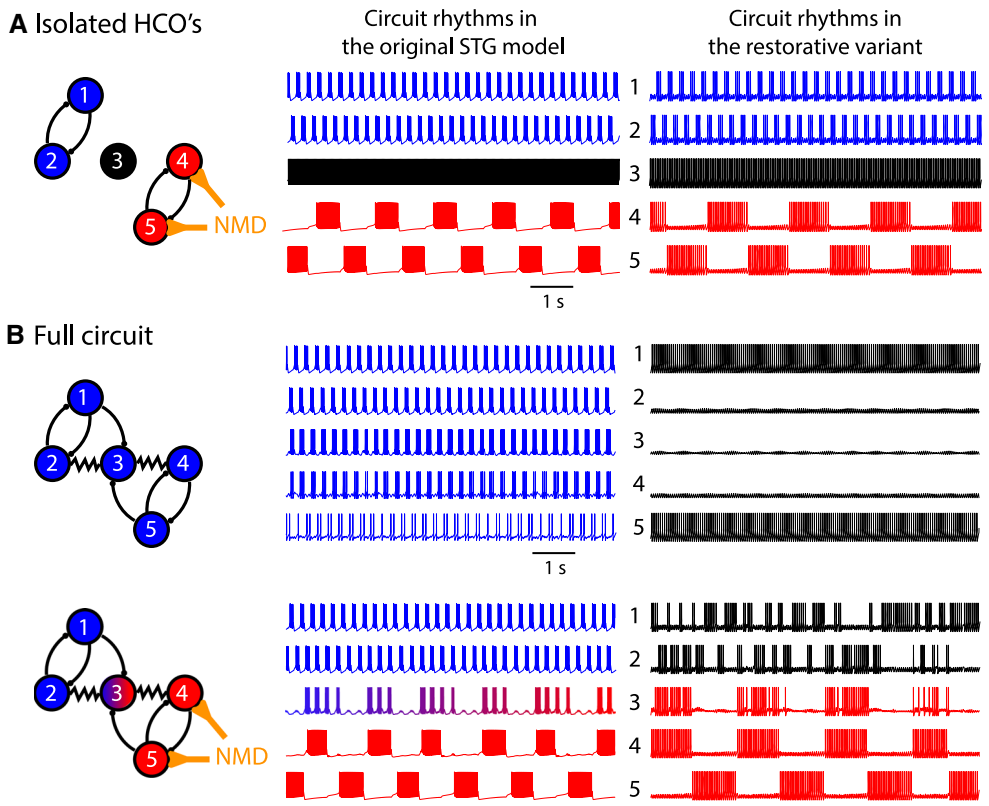

Fig. 1 Only the circuits that include a cellular slow negative conductance have robust rhythms modulated by connectivity changes and external inputs. Left, circuit connectivity diagram for **a** isolated half-center oscillators (HCOs) and **b** full connectivity with or without modulatory input. Filled circles represent neurons, which are numbered from 1 to 5. Black curves with rounded heads represent inhibitory connections. Thick orange curves represent active neuromodulatory (NMD) pathways targeting neurons 4 and 5. Resistor symbols represent electrical synaptic connections. Neurons that are involved in a fast rhythm are highlighted in blue, neurons that are involved in a slow rhythm are highlighted in red, and neurons that are not involved in a circuit rhythm are highlighted in black. Center and right membrane potential variations over time for neurons 1–5 (from top to bottom). Circuits in the left column include a slow negative conductance and are weakly connected. Circuits on the right do not include a slow negative conductance and require strong connectivity. A comparison between center and right traces shows that only circuits that include a cellular slow negative conductance allow for coexisting fast and slow rhythms (color figure online)

Secondly, we analyzed the robustness and possible coexistence of the two HCO rhythms in the five-neuron model (Fig. 1b) when HCO rhythms rely on either the cellular or circuit mechanism. As described above, the only difference between the two configurations is the calcium current activation time constant and the synaptic connection strength. This ensures that the cells are only differed by the presence or absence of sources of a slow negative conductance. In particular, their *static* properties such as membrane input resistance or neuron IV curve are identical. In the isolated HCOs (Fig. 1a), both the cellular or circuit mechanisms can produce qualitatively similar circuit rhythms in terms, for instance, of period and duty cycle. In both cases, the slow rhythm can be turned ON by the presence of a neuromodulator (NMD) that increases calcium channel densities. However, the two mechanisms show very different robustness properties when involved in the larger circuit (Fig. 1b).

The cellular mechanism produces HCO rhythms that are robust to changes in circuit connectivity and modulatory state of the slow HCO. With the slow rhythm turned off, the fast HCO rhythm is barely affected by its interconnection with the other neurons in the circuit and even propagates throughout the circuit by engaging the remaining neurons of the circuit in the fast rhythm (Fig. 1b, top center). The non-rhythmic neurons are entrained by the robust HCO rhythm. Modulating the slow HCO turns the slow rhythm ON without disrupting the fast rhythm, and both rhythms coexist at the level of the hub neuron (Fig. 1b, bottom center). Such robust switches in circuit activity are reminiscent of what is observed in the STG, both in experimental (Marder and Bucher 2007) and computational (Gutierrez et al. 2013) studies, as well as in other central pattern generators (Harris-Warrick 2011).

The circuit mechanism, on the other hand, produces HCO rhythms that are strongly affected by the full, five-neuron

circuit interconnection. With the slow rhythm turned off, the rhythm generated by the fast HCO does not survive its interconnection with the other neurons in the circuit even for relatively weak connectivity (in the example shown in Fig. 1b, top right, the connections to the hub neuron are ten times weaker than the connections within the HCOs, whereas they are of similar amplitude in the original STG model). In this case, the non-rhythmic neurons disrupt the HCO activity instead of being entrained by it. Maintaining the HCO rhythm requires to isolate the HCO sub-circuit by using extremely weak connections to the hub neuron, and there is no propagation of the rhythm throughout the circuit. Modulating the slow HCO turns the slow rhythm ON but results in some erratic behaviors in the fast neurons (Fig. 1b, bottom right). Fast and slow rhythms do not coexist robustly within the same circuit.

These results indicate that, although both cellular and circuit mechanisms can generate rhythms in simple circuit configurations, the cellular mechanism, which relies on the modulation of cellular slow negative conductances, is required for the robustness and coexistence of rhythms in larger connectivity diagrams. This highlights the important role played by slow regenerative channels for the generation and modulation of circuit rhythms in central pattern generators.

2.2 In spite of a fixed connectivity, cellular control of the slow negative conductances orchestrates the circuit rhythms

The previous section showed that circuit rhythms created by symmetrical HCOs could robustly coexist within a more complex structural connectome if they relied on the presence of a slow negative conductance at the cellular level. Single rhythms could, however, still be generated in the full structural connectome using strong connectivity between restorative neurons in this specific setup. In this section, we further explore the robustness and rhythmic capabilities of both mechanisms in circuits without any predefined structure in neuronal dynamics and synaptic connection strength. To this end, we simulated fifty different circuits by picking random voltage-gated current densities and random synaptic connection strengths (all were randomly picked in a range $[\bar{g}_c - 25\%, \bar{g}_c + 25\%]$ following a uniform distribution, where $\bar{g}_c$ is a central value that was chosen for each current following the results presented in Fig. 1). Furthermore, for each defined cellular and circuit configuration, several neuromodulatory configurations were simulated, where different neuromodulatory configurations are distinguished by different subsets of neuromodulated neurons.

In the absence of a slow negative conductance at the cellular level, breaking network symmetry and increasing cellular heterogeneity results in the incapacity to generate any circuit rhythm for any of the fifty randomly picked parameter sets and neuromodulatory configurations, even with strong network connectivity. The reason is that, in the absence of a slow negative conductance at the cellular level, circuit rhythms require a high degree of symmetry in the synaptic interconnections, which happens with low probability in large circuits with randomly distributed parameters. We do not show any quantitative result here, but identical observations have been reported in variable circuits and heterogeneous networks in Dethier et al. (2015) and Drion et al. (2018).

On the other hand, breaking network symmetry and increasing cellular heterogeneity in the presence of slow negative conductance at the cellular level revealed the ability of a fixed structural connectome to generate rich and diverse circuit rhythms or combinations of circuit rhythms. An illustrative example of this ability is provided in Fig. 2. The figure shows the activity of one of the circuits obtained by random variations of the model parameters in 5 different neuromodulatory states. All parameters, in particular voltage-gated and synaptic current densities, are identical in all states except for neuron calcium channel densities, which are under the control of external neuromodulators; hence, the structural connectome is identical in each state. In the absence of any neuromodulatory input, the slow negative conductance is shut down in all neurons and the circuit exhibits no rhythmic activity (Fig. 2, top). However, activating neuromodulatory pathways turns ON circuit rhythms of variable types depending on the set of neurons that are targeted by neuromodulators. In the provided example, the fixed structural connectome could exhibit either two coexisting fast and slow rhythms, a slow three-neuron rhythm, a fast three-neuron rhythm, or a global network rhythm for 4 different neuromodulatory states (Fig. 2, from second to bottom).

We performed a *functional connectivity* experiment on the toy circuit of Fig. 2 left. We low-pass-filtered membrane potential traces and measured the cross-covariance between nodes in the circuit. This provides a black box representation of the effective connectivity, or "functional connectome." The results are reported in Fig. 2 right, with thicker lines corresponding to higher cross-covariance. The rhythmic state of the circuit is trustfully reflected in the measured functional connectome. For instance, in the fast (resp. slow) three-neuron rhythm state the functional connectivity highlights the underlying three-neuron core. Both the coexistence of the fast and slow rhythms and the global rhythm lead to a connected functional connectivity graph. The quantitative difference is that the main connecting core is the neuronal triple 1–3–5 in the case of coexistence of fast and slow rhythms and the triple 2–3–4 in the case of the global rhythm.

The simple experiment in Fig. 2 highlights a fundamental fact. A fixed synaptic interconnection topology, with fixed synaptic connection strengths, is able to support a rich dic-

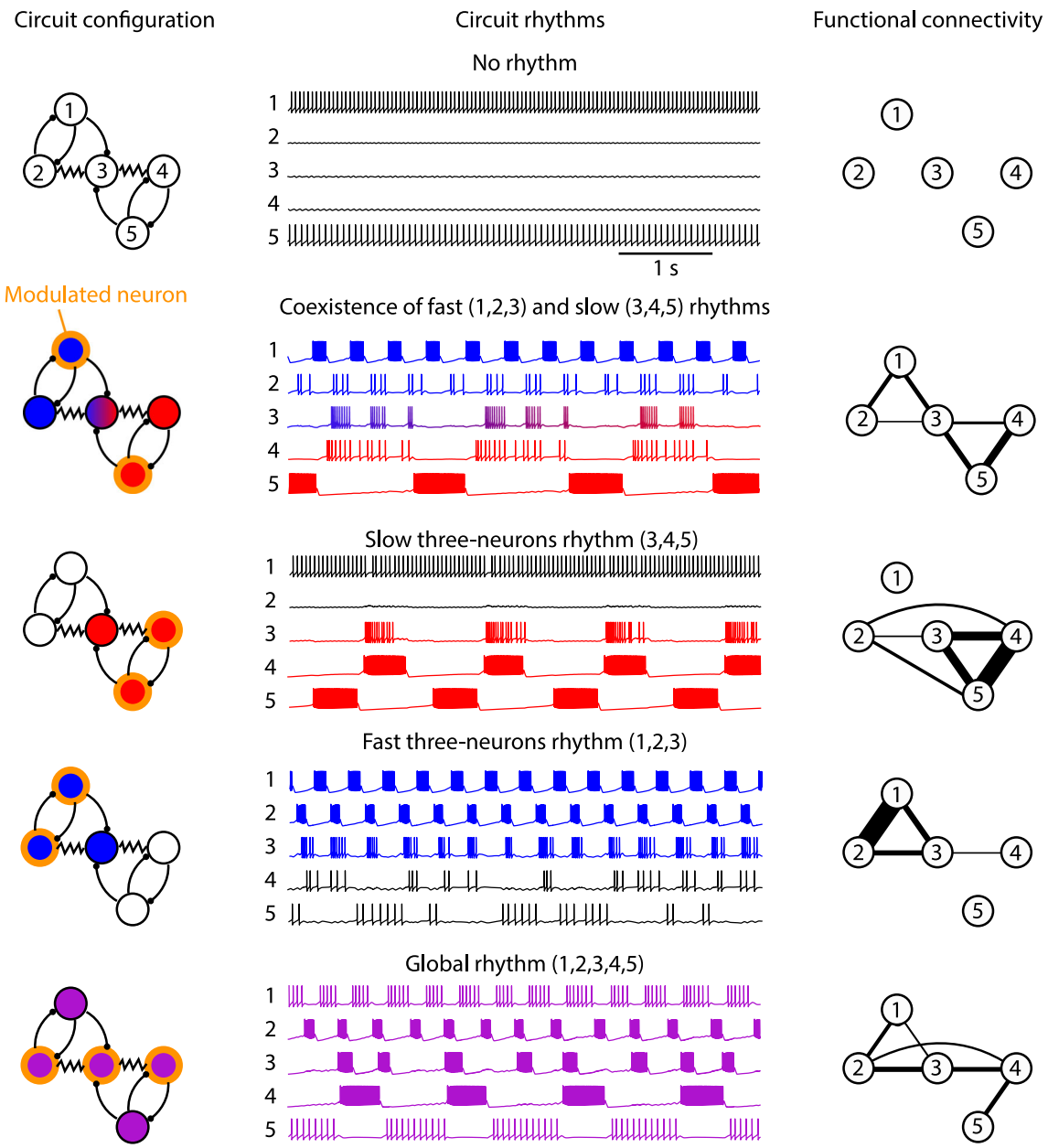

Fig. 2 Modulating the slow negative conductances of specific neurons selects different circuit rhythms and functional connectivities exist in spite of a fixed synaptic connectivity. Left, circuit connectivity diagrams. Filled circles represent neurons, which are numbered from 1 to 5. Black curves with rounded heads represent inhibitory connections. Resistor symbols represent electrical synaptic connections. Neurons with thick orange edges are subject to neuromodulatory inputs that increase the voltage-gated calcium channel density. Center, membrane potential variations over time for neurons 1–5 (from top to bottom) in the different modulatory configurations. Synaptic connections are identical in all cases. Neurons are colored in blue when they participate in the fast rhythm, in red when they participate in the slow rhythm, in purple when they participate in a global rhythm, and in black when they do not participate in the circuit rhythm. Right, functional connectome in the different modulatory configurations. Line thickness is proportional to the maximum of the cross-covariance function between voltages after low-pass filtering through the transfer function $H(s) = \frac{1}{30s+1}$. No line was drawn if this maximum was lower than 10 mV^2. See methods for more details (color figure online)

tionary of possible functional connectivity motifs, provided that tunable slow negative conductances are available at the cellular level.

Figure 2 only shows a few examples of the many network activities that can be exhibited by the circuit with fixed synaptic connections. But in a five-cell circuit and considering that each neuron can switch between two states (slow negative conductance off vs slow negative conductance on), the circuit can potentially reach $2^5 = 32$ different neuromodulatory states, each potentially resulting in its own specific circuit rhythm or combination of circuit rhythms. Considering the more physiological assumption that cellular slow negative conductances can be modulated in a continuous way, depending on neuromodulator concentration, for instance, further enriches the rhythmic capabilities of the circuit. Furthermore, rhythms that rely on the cellular mechanism being robust to changes in intrinsic parameters that do not affect the slow negative conductance, each neuromodulatory state can specifically be regulated by targeting voltage-gated currents that are not the principal sources of a slow negative conductance. Finally, modulation of synaptic connection (not considered here) adds a further layer of rhythm regulation that is compatible with the slow negative conductance switch.

2.3 Simple modeling of circuit rhythm modulation

Detailed neuron conductance-based models have the advantage of closely relating to physiology. They, however, can rapidly grow in dimension as further details about the neuron under study are taken into consideration. They often contain tens to hundreds of cell specific parameters, most of which are unknown, and model behavior can be highly sensitive to changes in many of them (Goldman et al. 2001; Prinz et al. 2003), making the parametrization of a conductance-based model an arduous case-by-case task. Results obtained using one specific conductance-based model are therefore often highly dependent on model specifics, hence difficult to generalize.

So far, we have shown that a change in one single parameter in a specific neuron conductance-based model that contains about a hundred different parameters can disrupt the whole control of the rhythmic circuit. This parameter controls the activation kinetics of the two calcium currents of the model, which are the only two sources of a slow negative conductance in the model. We concluded that switching slow negative conductance on and off at the cellular level was key to the robustness of rhythms at the circuit level. In order to further establish the generality of these results, we reproduced the previous computational experiments using a simple, hybrid model that captures the core dynamics of arbitrary conductance-based models. The simple model reads

$$\begin{aligned} \dot{V} &= V^2 - x_s^2 + bVx_s - g_s x_s - g_u x_u + I_{app} \\ \dot{x_s} &= \varepsilon_s(a_s V - x_s) \\ \dot{x_u} &= \varepsilon_u(a_u V - x_u), \end{aligned} \tag{1}$$

where V is the (adimensionalized) membrane potential, x_s a slow recovery variable, and x_u an ultraslow recovery variable ($\varepsilon_s >> \varepsilon_u$). V and x_s are reset to V_{reset} and $x_{s,reset}$, respectively, each time V crosses a threshold value V_{th}. In Eq. (1), the term $V^2 - x_s^2 + bVx_s$ is based on the local normal form of a transcritical bifurcation, which has been shown to organize the transition between *restorative excitability*, characterized by the absence of a slow negative conductance, and *regenerative excitability*, characterized by the presence of a slow negative conductance (Drion et al. 2012; Franci et al. 2013). In our model, this transition is controlled by the parameter g_s, which models in the adimensional model (1) the amplitude and sign of the slow conductance. This gain captures the role played by the slowly activating calcium currents in the conductance-based model used above.

The effect of g_s on model excitability is illustrated in Fig. 3a. The figure shows model response to short and long-lasting pulses of depolarizing and hyperpolarizing current for a positive or negative value of g_s (i.e., in the absence or presence of a slow negative conductance). All other parameters are strictly identical, expect for a steady current that decouples the value of g_s and model excitation state (see Methods). For positive g_s, the model shows the signatures of *restorative excitability*: A short pulse of depolarizing current induces a single spike, and a long-lasting pulse induces sustained spiking whose frequency depends on the amplitude of the depolarizing current (Fig. 3a, left). Such responses are reminiscent of already available simple neuron models. For negative g_s, the model response strongly differs and shows the signatures of *regenerative excitability*: A short pulse of depolarizing current induces a burst of spikes, a long-lasting pulse of moderate amplitude induces bursting, and a long-lasting pulse of large amplitude induces sustained spiking that can be temporarily interrupted by a short hyperpolarizing pulse (Fig. 3a, right).

Figure 3b shows the circuit rhythm generated by the interconnection of the simple models in the two modulatory states considered in Fig. 1b. Both the connectivity diagram and synapse models are identical to the ones used in the previous sections. In the absence of a slow negative conductance in neurons 4 and 5 (i.e., neuromodulatory inputs are shut down), the fast HCO rhythm generated by neurons 1 and 2 robustly spreads throughout the circuit up to neurons 3 and 4 (Fig. 3b, top). Turning ON the slow negative conductance in neurons 4 and 5 induces the generation of a slow HCO rhythm that

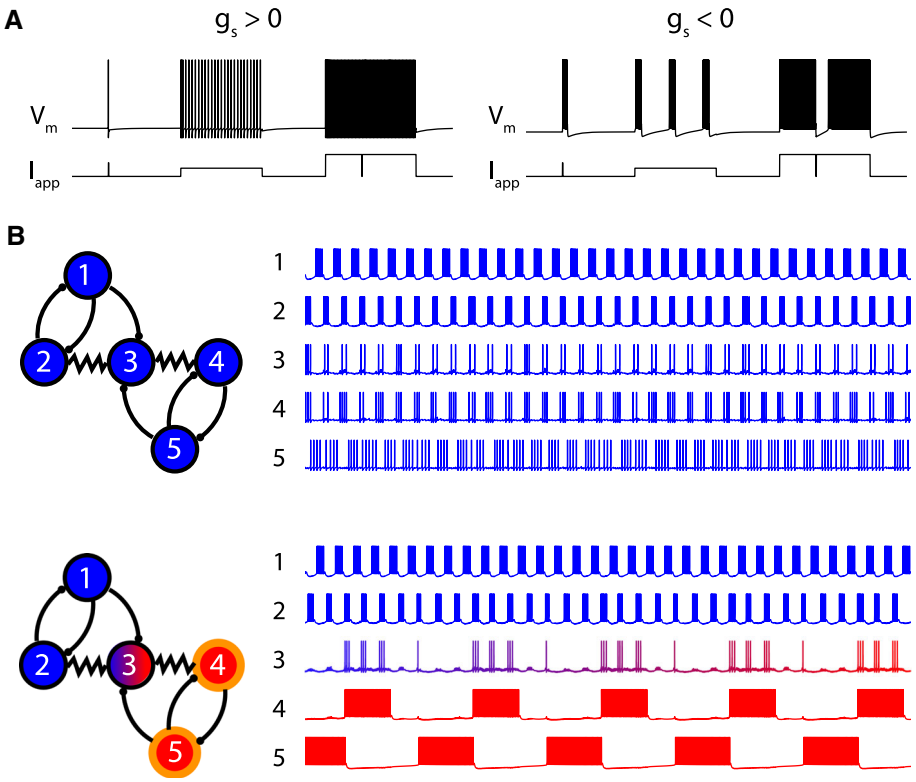

Fig. 3 Coexistence of rhythms in a simplified computational model that captures the role of the slow negative conductances via the single conductance parameter g_s. **a** Responses of the hybrid neuron model (V_m, top) to pulses of depolarizing and hyperpolarizing current (I_{app}, bottom) when the slow conductance around resting potential is positive ($g_s > 0$, left) or negative ($g_s < 0$, right). All other parameters are identical, except for a steady current that decouples the value of g_s and model excitation state. **b** Left, circuit connectivity diagrams. Filled circles represent neurons, which are numbered from 1 to 5. Black curves with rounded heads represent inhibitory connections. Resistor symbols represent electrical coupling. Tick orange curves represent active neuromodulatory pathways targeting neurons 4 and 5. **b** Right, membrane potential variations over time of each neuron in the absence (top) or presence (bottom) of a neuromodulatory input to neurons 4 and 5. Neurons are colored in blue when they participate in the fast rhythm, and in red when they participate in the slow rhythm (color figure online)

coexists with the fast rhythm, and neuron 3 is involved in both the fast and the slow rhythms.

These results show that, although the simple model lacks most of the specific details of the conductance-based model, it is sufficient to capture the cellular mechanism necessary to the robust control of the circuit rhythms. The significance of such results is twofold. On the one hand, they demonstrate the critical role played by the cellular slow negative conductance for the generation and control of robust circuit rhythms. On the other hand, they show that robust circuit rhythmic activity can be studied using simple neuron models provided that these models have the ability to control the absence or presence of a slow negative conductance at the cellular level. Several such models have been recently developed and studied mathematically (Drion et al. 2012; Franci et al. 2012, 2014; Pottelbergh et al. 2018).

3 Discussion

3.1 Decoupling the rhythm selection from the rhythm regulation

We have highlighted the role of a slow negative cellular conductance in the robust control of circuit rhythms. This property endows each neuron with two distinct modes of excitability: The neuron is burst excitable when the slow negative conductance is on and spike excitable when the slow negative conductance is off. This switching mechanism is simple. It exists in any neuron that includes slowly activating calcium currents, and its external control only requires a neuromodulator that controls channel density. Recent results suggest experimental evidence of neuromodulators that modulate the intrinsic burstiness of the neurons, and participate in the control of the circuit rhythm (McLean et al. 2008; Berkowitz et al. 2010; Zhong et al. 2011; White and Nusbaum 2011). Such experiments are consistent with the view that the circuit rhythm is modulated via intrinsic rather than

synaptic conductances. The cellular switch does not tune a rhythm. It only controls the participation of a given node in the network rhythm.

The cellular mechanism endows the circuit with a selection mechanism: Many functional connectomes can be selected from a given structural connectome, that is, a given configuration of synaptic and electrical couplings. Shaping the structural connectome has profound effect on the circuit rhythm (Gutierrez et al. 2013). Complementary to this structural modulation, cellular neuromodulators can selectively control the participation of each node in the functional connectome. Given a fixed structural connectome, different rhythms can be turned on and off by acting at the cellular level.

The selection of a functional connectome is largely decoupled from the tuning of the circuit rhythm in that particular configuration. The circuit rhythm results from specific transition times between high and low firing activity of the neurons, and the functional connectome only constrains the phase properties of those transition times. The precise tuning of the transition times involves both the intrinsic properties of the neurons and the synaptic and electrical couplings. In that sense, the rhythm regulation is largely decoupled from the rhythm selection.

This decoupling is required by the different timescales involved in circuit regulation. The behavioral timescale of an animal requires control actions within hundreds of milliseconds to seconds. Such rapid modulation is not compatible with synaptic plasticity. But it is compatible with the action of neuromodulators that select different functional connectomes. There is increasing experimental evidence that neuromodulation plays a major role in shaping the functional connectome (Marder 2012; Bargmann and Marder 2013). This conclusion probably extends to many more spatial scales, from small circuits to whole brain activity (Haider and McCormick 2009; Mennes et al. 2012; Ekman et al. 2012; Francis et al. 2018; Honey et al. 2007).

The tuning of circuit rhythms occurs over a broad range of timescales that include, for instance, the slower timescale of synaptic plasticity. While the tuning properties of the circuit rhythms have not been studied in detail in the present paper, it is rather intuitive that a discrete selection mechanism considerably enriches the tunability of a circuit. Our previous work (Dethier et al. 2015) showed how the slow negative conductance of neurons contributes to robustness and tunability of a half-center oscillator, which is directly relevant to the circuits studied in the present paper. Our recent work (Drion et al. 2018) shows similar conclusions in much larger populations of neurons that switch between an active and oscillatory state.

3.2 A cellular property that matters at the circuit level

The slow negative conductance emphasized in this paper is not the property of a particular ionic current. It is a property of the total current–voltage relationship of the neuron, and it can be regulated by the expression of many different channels. It has a specific signature in a voltage clamp experiment (see for instance the discussion in Franci et al. 2018) and can be easily assessed in a detailed conductance-based model (see for instance Franci et al. 2013). This property is also distinct from the rebound mechanism property necessary for the anti-phase rhythm of a half-center oscillator (Dethier et al. 2015). It is in fact a property that seems to have received little attention until recently (Drion et al. 2012).

The question of which cellular details must be included in the computational model of a circuit is often a matter of debate: Detailed cellular models facilitate the biophysical interpretation of the model properties, but detailed cellular models are impractical in circuit studies because they result in large dimensional models with many parameters to tune rather arbitrarily. Circuit models that use a simplified neuronal model are thus preferred, but they raise the question of which details of the full model must be retained.

Popular simplified neuronal models include the Hodgkin–Huxley model, planar reductions in Hodgkin–Huxley model (e.g., Fitzhugh–Nagumo model), or linear and quadratic integrate-and-fire models. None of those models possess the cellular property emphasized in this paper. We refer the interested reader to Drion et al. (2012) and Pottelbergh et al. (2018) for a detailed analysis of why those models do not include a slow negative conductance and how to modify them to account for this specific property.

We have illustrated the control properties of the STG circuit by using a detailed conductance-based model for each neuron, but we have also shown that the same control mechanism can be reproduced in a reduced model that uses highly simplified equations for each neuron. This simplification underlines that the proposed mechanism does not result from the biological details of neuronal models but only from the slow negative conductance property of the total current–voltage relationship of each neuron. It is therefore conceivable to include this property in simple models of artificial central pattern generators that could inform the design and control principles of rhythmic machines. Such models could, for instance, expand the control principles grounded in phase models of central pattern generators in the design of artificial locomotion (Ijspeert et al. 2007).

4 Methods

4.1 Neuron conductance-based model

All simulations and analyses were performed using the Julia programming language. The Julia code is freely available at http://www.montefiore.ulg.ac.be/~guilldrion/Files/DFS2018-code.zip.

Figures 1 and 2 are generated using the STG model described in (Liu et al. 1998). The model follows the voltage equation

$$C\dot{V} = -I_{\text{ion}} + I_{\text{app}},$$

where V is neuron membrane potential, C is the membrane capacitance, I_{ion} represents ionic currents, and I_{app} represents an externally applied current. Ionic currents are composed of a leak current I_{leak}, a transient sodium current I_{Na}, a T-type calcium current $I_{\text{Ca,T}}$, a S-type calcium current $I_{\text{Ca,S}}$, a delayed rectifier potassium current $I_{\text{K,DR}}$, a transient potassium current I_{A}, a calcium-activated potassium current $I_{\text{K,Ca}}$, and a hyperpolarization-activated cation current I_H. Fixed parameters used in the simulations were as follows: $C = 1\,\mu\text{F}\cdot\text{cm}^{-2}$, $V_{\text{Na}} = 50\,\text{mV}$, $V_K = -80\,\text{mV}$, $V_{Ca} = 80\,\text{mV}$, $V_{\text{leak}} = -50\,\text{mV}$, and $\bar{g}_{\text{leak}} = 0.01\,\text{mS}\,\text{cm}^{-2}$.

In Fig. 1, variable parameters were as follows. Neurons 1 and 2: $\bar{g}_{\text{Na}} = 600\,\text{mS}\,\text{cm}^{-2}$, $\bar{g}_{\text{Ca,T}} = 3\,\text{mS}\,\text{cm}^{-2}$, $\bar{g}_{\text{Ca,S}} = 8\,\text{mS}\,\text{cm}^{-2}$, $\bar{g}_{\text{A}} = 50\,\text{mS}\,\text{cm}^{-2}$, $\bar{g}_{\text{K,DR}} = 90\,\text{mS}\,\text{cm}^{-2}$, $\bar{g}_{\text{K,Ca}} = 60\,\text{mS}\,\text{cm}^{-2}$. Neuron 3: $\bar{g}_{\text{Na}} = 600\,\text{mS}\,\text{cm}^{-2}$, $\bar{g}_{\text{Ca,T}} = 3\,\text{mS}\,\text{cm}^{-2}$, $\bar{g}_{\text{Ca,S}} = 2\,\text{mS}\,\text{cm}^{-2}$, $\bar{g}_{\text{A}} = 50\,\text{mS}\,\text{cm}^{-2}$, $\bar{g}_{\text{K,DR}} = 90\,\text{mS}\,\text{cm}^{-2}$, $\bar{g}_{\text{K,Ca}} = 30\,\text{mS}\,\text{cm}^{-2}$. Neurons 4 and 5: $\bar{g}_{\text{Na}} = 600\,\text{mS}\,\text{cm}^{-2}$, $\bar{g}_{\text{A}} = 50\,\text{mS}\,\text{cm}^{-2}$, $\bar{g}_{\text{K,DR}} = 90\,\text{mS}\,\text{cm}^{-2}$, $\bar{g}_{\text{K,Ca}} = 60\,\text{mS}\,\text{cm}^{-2}$, and $\bar{g}_{\text{Ca,T}} = 1\,\text{mS}\,\text{cm}^{-2}$, $\bar{g}_{\text{Ca,S}} = 1\,\text{mS}\,\text{cm}^{-2}$ (unmodulated state) or $\bar{g}_{\text{Ca,T}} = 3\,\text{mS}\,\text{cm}^{-2}$, $\bar{g}_{\text{Ca,S}} = 8\,\text{mS}\,\text{cm}^{-2}$ (modulated state). In addition, a parameter $\tau_{\text{mK,Ca}}$ multiplying the calcium-activated potassium current time constant was added and set to 1 for neurons 1, 2, and 3 (fast rhythm) and set to 20 for neurons 4 and 5 (slow rhythm).

In Fig. 2, maximal conductances were randomly picked in a range $[\bar{g}_{\text{c}} - 25\%, \bar{g}_{\text{c}} + 25\%]$ following a uniform distribution, where $\bar{g}_{\text{c}}$ is a central value that was chosen for each current. These central values were $\bar{g}_{\text{Na,c}} = 600\,\text{mS}\,\text{cm}^{-2}$, $\bar{g}_{\text{A,c}} = 50\,\text{mS}\,\text{cm}^{-2}$, $\bar{g}_{\text{K,DR,c}} = 90\,\text{mS}\,\text{cm}^{-2}$, $\bar{g}_{\text{K,Ca,c}} = 60\,\text{mS}\,\text{cm}^{-2}$. For the unmodulated state, $\bar{g}_{\text{Ca,T,c}} = 1\,\text{mS}\,\text{cm}^{-2}$, $\bar{g}_{\text{Ca,S,c}} = 3\,\text{mS}\,\text{cm}^{-2}$. For the modulated state, $\bar{g}_{\text{Ca,T,c}} = 3\,\text{mS}\,\text{cm}^{-2}$, $\bar{g}_{\text{Ca,S,c}} = 8\,\text{mS}\,\text{cm}^{-2}$. $\tau_{\text{mK,Ca}}$ was randomly picked in a range [5.5, 24.5].

Finally, a parameter τ_{mCa} multiplying both calcium current time constants was added and set to 1 for the *original model* and to 0.1 to create the *restorative variant*.

4.2 Neuron hybrid model

The neuron hybrid model used in Fig. 3 is based on the normal form of the transcritical bifurcation (Drion et al. 2012; Franci et al. 2013). It reads

$$\begin{aligned}
\dot{V} &= V^2 - x_{\text{s}}^2 + bVx_{\text{s}} - g_{\text{s}}x_{\text{s}} - g_{\text{u}}x_{\text{u}} + I_{\text{ss}} + I_{\text{app}}\\
\dot{x_{\text{s}}} &= \varepsilon_{\text{s}}(a_{\text{s}}V - x_{\text{s}})\\
\dot{x_{\text{u}}} &= \varepsilon_{\text{u}}(a_{\text{u}}V - x_{\text{u}}),
\end{aligned}$$

where V is the membrane potential, x_{s} a slow recovery variable, x_{u} an ultraslow recovery variable ($\varepsilon_{\text{s}} >> \varepsilon_{\text{u}}$), and I_{app} an externally applied current. $I_{ss} = (-(-2V_{\text{ss}}(1 - a_{\text{s}}^2 + a_{\text{s}}b) - a_{\text{s}}(g_{\text{s}} + g_{\text{u}}))^2 + a_{\text{s}}^2(g_{\text{s}} + g_{\text{u}})^2)/(4(1 - a_{\text{s}}^2 + a_{\text{s}}b))$ is a steady current that decouples the value of g_{s} and model excitation state at V_{ss} (set to -2). To make the value of the membrane potential similar to the one of the conductance-based model, the membrane potential V was shifted by $-70\,\text{mV}$. This shift is only necessary to ensure similar synaptic current activation with both models. Finally, the reset rule reads

$$\begin{aligned}
\text{if } V > V_{\text{th}} \quad \text{then} \quad & V \leftarrow V_{\text{reset}}\\
& x_{\text{s}} \leftarrow x_{\text{s,reset}}\\
& x_{\text{u}} \leftarrow x_{\text{u}} + \Delta x_{\text{u}}.
\end{aligned}$$

The non-tunable parameters were set as follows: $b = -2$, $a_{\text{s}} = a_{\text{u}} = 0.1$, $V_{\text{reset}} = 40$, $x_{\text{s,reset}} = 30$, and $\Delta x_{\text{u}} = 20$. The tunable parameters were neuron dependent. Neurons 1 and 2: $g_{\text{s}} = -30$, $g_{\text{u}} = 2$, $I_{\text{app}} = 40$, $\varepsilon_{\text{s}} = 1$, $\varepsilon_{\text{u}} = 0.1$. Neuron 3: $g_{\text{s}} = 0$, $g_{\text{u}} = 1$, $I_{\text{app}} = 0$, $\varepsilon_{\text{s}} = 1$, $\varepsilon_{\text{u}} = 0.1$. Neurons 4 and 5: $g_{\text{s}} = 0$ (unmodulated state) or $g_{\text{s}} = -30$ (modulated state), $g_{\text{u}} = 0.2$, $I_{\text{app}} = 60$, $\varepsilon_{\text{s}} = 1$, $\varepsilon_{\text{u}} = 0.01$.

4.3 Synaptic connections

Neurons were connected through chemical inhibitory synapses and electrical synapses. Synaptic currents were added to the following voltage equation

$$C\dot{V} = -I_{\text{ion}} + I_{\text{app}} - I_{\text{syn}} - I_{\text{el}}$$

in case of the conductance-based model, and

$$\dot{V} = V^2 - x_{\text{s}}^2 + bVx_{\text{s}} - g_{\text{s}}x_{\text{s}} - g_{\text{u}}x_{\text{u}} + I_{ss} + I_{\text{app}} - I_{\text{syn}} - I_{\text{el}}$$

in case of the hybrid model, where I_{syn} represents the chemical synaptic current and I_{el} the electrical synaptic current. The electrical synaptic current was modeled following the equation $I_{\text{el}} = \bar{g}_{\text{el}}(V_{\text{post}} - V_{\text{pre}})$, where $\bar{g}_{\text{el}}$ is the maximal conductance of the electrical synapse, V_{post} is the membrane

potential of the postsynaptic neuron, and V_{pre} is the membrane potential of the presynaptic neuron. Electrical synapses were considered to transmit in both directions. The chemical synaptic current was modeled following the equation $I_{\text{syn}} = \bar{g}_{\text{syn}} s (V_{\text{post}} - V_{\text{syn}})$, where $\bar{g}_{\text{syn}}$ is the maximal conductance of the chemical synapse, V_{post} is the membrane potential of the postsynaptic neuron, and V_{syn} is the synaptic reversal potential (set to -75 mV in all simulations). s is the synaptic activation variable that depends on the membrane potential of the presynaptic neuron following the equation

$$\tau_{\text{s}} \dot{s} = s_\infty(V_{\text{pre}}) - s,$$

where τ_{s} is the synaptic activation time constant, which was set to 10 ms when using the conductance-based models and to 1 ms when using the hybrid model (although the dimension has little meaning in the latter case). $s_\infty(V_{\text{pre}})$ is the steady-state activation curve defined by

$$s_\infty = \begin{cases} 0 & \text{if} \quad V_{\text{pre}} < V_{\text{th,syn}}; \\ \tanh((V_{\text{pre}} - V_{\text{th,syn}})/V_{\text{slope}}) & \text{if} \quad V_{\text{th,syn}} \geq V_{\text{th,syn}}, \end{cases}$$

where $V_{\text{th,syn}}$ was set to -50 mV and V_{slope} to 10 mV.

In Fig. 1a, center, the following synaptic maximal conductances were used ($\bar{g}_{\text{syn}}^{i,j}$ represents the synaptic connection from neuron i to neuron j): $\bar{g}_{\text{syn}}^{1,2} = \bar{g}_{\text{syn}}^{2,1} = \bar{g}_{\text{syn}}^{4,5} = \bar{g}_{\text{syn}}^{5,4} = 0.2\,\text{mS cm}^{-2}$, $\bar{g}_{\text{syn}}^{1,3} = \bar{g}_{\text{syn}}^{5,3} = \bar{g}_{\text{el}}^{2,3} = \bar{g}_{\text{el}}^{3,2} = 0\,\text{mS cm}^{-2}$. In Fig. 1a, right, the nonzero maximal synaptic conductances were ten times stronger: $\bar{g}_{\text{syn}}^{1,2} = \bar{g}_{\text{syn}}^{2,1} = \bar{g}_{\text{syn}}^{4,5} = \bar{g}_{\text{syn}}^{5,4} = 2\,\text{mS cm}^{-2}$. In Fig. 1b, synaptic maximal conductances were as in Fig. 1a except for $\bar{g}_{\text{syn}}^{1,3} = \bar{g}_{\text{syn}}^{5,3} = 0.2\,\text{mS cm}^{-2}$ and $\bar{g}_{\text{el}}^{2,3} = \bar{g}_{\text{el}}^{3,2} = 0.05\,\text{mS cm}^{-2}$.

In Fig. 2, synaptic maximal conductances were randomly picked in a range $[\bar{g}_{\text{c}} - 25\%, \bar{g}_{\text{c}} + 25\%]$ following a uniform distribution, where $\bar{g}_{\text{c}}$ is a central value chosen as follows: $\bar{g}_{\text{syn,c}}^{1,2} = \bar{g}_{\text{syn,c}}^{2,1} = \bar{g}_{\text{syn,c}}^{4,5} = \bar{g}_{\text{syn,c}}^{5,4} = \bar{g}_{\text{syn,c}}^{1,3} = \bar{g}_{\text{syn,c}}^{5,3} = 0.01\,\text{mS cm}^{-2}$ and $\bar{g}_{\text{el,c}}^{2,3} = \bar{g}_{\text{el,c}}^{3,2} = 0.02\,\text{mS cm}^{-2}$.

In Fig. 3, the following synaptic maximal conductances were used: $\bar{g}_{\text{syn}}^{1,2} = \bar{g}_{\text{syn}}^{2,1} = \bar{g}_{\text{syn}}^{4,5} = \bar{g}_{\text{syn}}^{5,4} = \bar{g}_{\text{syn}}^{1,3} = \bar{g}_{\text{syn}}^{5,3} = 15$ and $\bar{g}_{\text{el}}^{2,3} = \bar{g}_{\text{el}}^{3,2} = 3$. These values are dimensionless.

4.4 Functional connectome

The functional connectome was computed by computing the cross-covariance between low-pass-filtered membrane potential time courses of pairs of neurons. The used filter transfer function was $H(s) = \frac{1}{30s+1}$. The maximum of the absolute value of the cross-covariance, computed through the `crosscov` function in the Julia StatsBase package, was extracted and used to build the functional connectome link weights.

References

Ashby R (1952) Design for a brain: the origin of adaptive behavior. Wiley, Oxford

Bargmann C, Marder E (2013) From the connectome to brain function. Nat Methods 10(6):483–490

Berkowitz A, Roberts A, Soffe S (2010) Roles for multifunctional and specialized spinal interneurons during motor pattern generation in tadpoles, zebrafish larvae, and turtles. Front Behav Neurosci 4:36

Bucher D, Taylor AL, Marder E (2006) Central pattern generating neurons simultaneously express fast and slow rhythmic activities in the stomatogastric ganglion. J Neurophysiol 95(6):3617–3632

Butera RJ, Rinzel J, Smith JC (1999) Models of respiratory rhythm generation in the pre-bötzinger complex. ii. Populations of coupled pacemaker neurons. J Neurophysiol 82(1):398–415

Dai Y, Jordan L (2010) Multiple patterns and components of persistent inward current with serotonergic modulation in locomotor activity-related neurons in Cfos-EGFP mice. J Neurophysiol 103(4):1712–1727

Daur N, Nadim F, Bucher D (2016) The complexity of small circuits: the stomatogastric nervous system. Curr Opin Neurobiol 41:1–7

Dethier J, Drion G, Franci A, Sepulchre R (2015) A positive feedback at the cellular level promotes robustness and modulation at the circuit level. J Neurophysiol 114:2472–2484

Dickinson P, Mecsas C, Marder E (1990) Neuropeptide fusion of two motor-pattern generator circuits. Nature 344(6262):155

Drion G, Franci A, Seutin V, Sepulchre R (2012) A novel phase portrait for neuronal excitability. PLoS ONE 7(8):e41,806

Drion G, Franci A, Dethier J, Sepulchre R (2015) Dynamic input conductances shape neuronal spiking. eNeuro. https://doi.org/10.1523/ENEURO.0031-14.2015

Drion G, Dethier J, Franci A, Sepulchre R (2018) Switchable slow cellular conductances determine robustness and tunability of network states. PLOS Comput Biol 14(4):e1006125

Ekman M, Derrfuss J, Tittgemeyer M, Fiebach C (2012) Predicting errors from reconfiguration patterns in human brain networks. Proc Natl Acad Sci USA 109(41):16,714–16,719

FitzHugh R (1961) Impulses and physiological states in theoretical models of nerve membrane. Biophys J 1(6):445

Franci A, Drion G, Sepulchre R (2012) An organizing center in a planar model of neuronal excitability. SIAM J Appl Dyn Syst 11(4):1698–1722

Franci A, Drion G, Seutin V, Sepulchre R (2013) A balance equation determines a switch in neuronal excitability. PLoS Comput Biol 9(5):e1003,040

Franci A, Drion G, Sepulchre R (2014) Modeling the modulation of neuronal bursting: a singularity theory approach. SIAM J Appl Dyn Syst 13(2):798–829

Franci A, Drion G, Sepulchre R (2018) Robust and tunable bursting requires slow positive feedback. J Neurophysiol 119(3):1222–1234. arXiv:1707.00664

Francis N, Winkowski D, Sheikhattar A, Armengol K, Babadi B, Kanold P (2018) Small networks encode decision-making in primary auditory cortex. Neuron 97(4):885–897

Gerstner W, Kistler W, Naud R, Paninski L (2014) Neuronal dynamics: from single neurons to networks and models of cognition. Cambridge University Press, Cambridge

Goldman MS, Golowasch J, Marder E, Abbott LF (2001) Global structure, robustness, and modulation of neuronal models. J Neurosci 21(14):5229–5238

Golomb D, Amitai Y (1997) Propagating neuronal discharges in neocortical slices: computational and experimental study. J Neurophysiol 78(3):1199–1211

Gordon I, Whelan P (2006) Monoaminergic control of cauda-equina-evoked locomotion in the neonatal mouse spinal cord. J Neurophysiol 96(6):3122–3129

Grillner S (2003) The motor infrastructure: from ion channels to neuronal networks. Nat Rev Neurosci 4(7):573–586

Gutierrez G, O'Leary T, Marder EE (2013) Multiple mechanisms switch an electrically coupled, synaptically inhibited neuron between competing rhythmic oscillators. Neuron 77(5):845–858

Haider B, McCormick D (2009) Rapid neocortical dynamics: cellular and network mechanisms. Neuron 62(2):171–189

Harris-Warrick R (2011) Neuromodulation and flexibility in central pattern generator networks. Curr Opin Neurobiol 21(5):685–692

Harris-Warrick R, Cohen A (1985) Serotonin modulates the central pattern generator for locomotion in the isolated lamprey spinal cord. J Exp Biol 116(1):27–46

Hill A, Hooser SV, Calabrese R (2003) Half-center oscillators underlying rhythmic movements. MIT Press, Cambridge, pp 507–510

Honey C, Kötter R, Breakspear M, Sporns O (2007) Network structure of cerebral cortex shapes functional connectivity on multiple time scales. Proc Natl Acad Sci USA 104(24):10,240–10,245

Ijspeert A (2014) Biorobotics: Using robots to emulate and investigate agile locomotion. Science 346(6206):196–203

Ijspeert A, Crespi A, Ryczko D, Cabelguen JM (2007) From swimming to walking with a salamander robot driven by a spinal cord model. Science 315(5817):1416–1420

Jordan L, Slawinska U (2011) Modulation of rhythmic movement: control of coordination, progress in brain research, vol 188. Elsevier, Amsterdam, pp 181–195

Liu Z, Golowasch J, Marder E, Abbott L (1998) A model neuron with activity-dependent conductances regulated by multiple calcium sensors. J Neurosci 18(7):2309–2320

Liu J, Akay T, Hedlund P, Pearson K, Jordan L (2009) Spinal 5-ht7 receptors are critical for alternating activity during locomotion: in vitro neonatal and in vivo adult studies using 5-ht7 receptor knockout mice. J Neurophysiol 102(1):337–348

Marder E (2012) Neuromodulation of neuronal circuits: back to the future. Neuron 76(1):1–11

Marder E, Bucher D (2001) Central pattern generators and the control of rhythmic movements. Curr Biol 11(23):R986–R996

Marder E, Bucher D (2007) Understanding circuit dynamics using the stomatogastric nervous system of lobsters and crabs. Annu Rev Physiol 69:291–316

Marder E, O'Leary T, Shruti S (2014) Neuromodulation of circuits with variable parameters: Single neurons and small circuits reveal principles of state-dependent and robust neuromodulation. Annu Rev Neurosci 37:329–347

Marder E, Goeritz M, Otopalik A (2015) Robust circuit rhythms in small circuits arise from variable circuit components and mechanisms. Curr Opin Neurobiol 31:156–163

McLean D, Masino M, Koh I, Lindquist W, Fetcho J (2008) Continuous shifts in the active set of spinal interneurons during changes in locomotor speed. Nat Neurosci 11(12):1419–1429

Mennes M, Kelly C, Colcombe S, Castellanos F, Milham M (2012) The extrinsic and intrinsic functional architectures of the human brain are not equivalent. Cereb Cortex 23(1):223–229

Meyrand P, Simmers J, Moulins M (1991) Construction of a pattern-generating circuit with neurons of different networks. Nature 351(6321):60

Pottelbergh TV, Drion G, Sepulchre R (2018) Robust modulation of integrate-and-fire models. Neural Comput 30(4):987–1011

Prinz A, Billimoria C, Marder E (2003) Alternative to hand-tuning conductance-based models: construction and analysis of databases of model neurons. J Neurophysiol 90(6):3998–4015

Rodriguez J, Blitz D, Nusbaum M (2013) Convergent rhythm generation from divergent cellular mechanisms. J Neurosci 33(46):18,047–18,064

Rubin JE, Terman D (2004) High frequency stimulation of the subthalamic nucleus eliminates pathological thalamic rhythmicity in a computational model. J Comput Neurosci 16(3):211–35

Terman D, Rubin JE, Yew AC, Wilson CJ (2002) Activity patterns in a model for the subthalamopallidal network of the basal ganglia. J Neurosci 22(7):2963–76

Weimann J, Marder E (1994) Switching neurons are integral members of multiple oscillatory networks. Curr Biol 4(10):896–902

White R, Nusbaum M (2011) The same core rhythm generator underlies different rhythmic motor patterns. J Neurosci 31(32):11,484–11,494

Zhong G, Sharma K, Harris-Warrick R (2011) Frequency-dependent recruitment of V2a interneurons during fictive locomotion in the mouse spinal cord. Nat Commun 2:274